BIAXIAL AND FAILURE PROPERTIES OF PASSIVE RAT MIDDLE CEREBRAL ARTERIES

by

Rahul Subhash Kunjir

A thesis submitted to the faculty of
The University of Utah
in partial fulfillment of the requirements for the degree of

Master of Science

Department of Mechanical Engineering

The University of Utah

May 2012

The University of Utah Graduate School

STATEMENT OF THESIS APPROVAL

The thesis of **Rahul Subhash Kunjir**

has been approved by the following supervisory committee members:

Kenneth L. Monson	, Chair	**12/14/11** Date Approved
Daniel O. Adams	, Member	**12/15/11** Date Approved
Donald S. Bloswick	, Member	**12/16/11** Date Approved

and by **Timothy A. Ameel** , Chair of

the Department of **Mechanical Engineering**

and by Charles A. Wight, Dean of The Graduate School.

ABSTRACT

Rodents are commonly used as test subjects in research on traumatic brain injury and stroke. However, study of rat cerebral vessel properties has largely been limited to pressure-diameter response within the physiological loading range. A more complete, multiaxial description is needed to guide experiments on rats and to appropriately translate findings to humans. Accordingly, we dissected seven rat middle cerebral arteries (MCAs) and subjected them to combined inflation and axial stretch tests around physiological loading conditions while in a passive state. The MCAs were finally stretched axially to failure. Responses in the axial and circumferential directions were relatively similar in contrast to previously reported behavior of human cerebral arteries. Failure stretch values were similar in rat and human vessels, but corresponding stress values for rats were considerably lower than those for humans. Differences between human and rat vessel properties should be considered in rat models of human cerebrovascular injury and disease.

To my parents,

Nirmala and Subhash Kunjir

TABLE OF CONTENTS

LIST OF FIGURES

Figure Page

ACKNOWLEDGEMENTS

I would like to thank my research advisor Dr. Kenneth Monson for his mentoring, and providing valuable guidance and motivation throughout this study. I would also like to thank Edward Bell for his assistance with conducting the experiments. This work was supported by grants from the National Institutes of Health (5K25HD048643) and the Department of Defense (W81XWH-08-1-0295).

CHAPTER 1

INTRODUCTION

Disruption of cerebral blood vessel function leads to stroke and is a common outcome of traumatic brain injury (TBI). In the United States, 52,000 deaths result from over 1.7 million cases of TBI annually (Faul, Xu et al. 2010); the number of deaths is over 140,000 per year for stroke (Lloyd-Jones, Adams et al. 2010). Total annual costs associated with TBI and stroke have been estimated at 60 (Faul, Xu et al. 2010) and 65.5 (Rosamond, Flegal et al. 2008) billion dollars, respectively.

1.1 Cerebrovascular Mechanics in Humans

Efforts to better prevent and treat cerebrovascular injury and disease are, in part, dependent upon a more complete understanding of vessel mechanics. This includes definition of blood vessel injury thresholds as well as characterization of relationships between applied forces and vessel function. Experiments on human cerebral vessels have revealed some characteristics of these tissues (Busby and Burton 1965; Scott, Ferguson et al. 1972; Hayashi, Nagasawa et al. 1980; Monson, Barbaro et al. 2008), but many questions remain, and the availability of human specimens is limited.

1.2 Cerebrovascular Mechanics in Rodents

Rodents are commonly used as models for both TBI and stroke (Hogestatt, Andersson et al. 1983; Hajdu and Baumbach 1994; Coulson, Chesler et al. 2002; Coulson, Cipolla et al. 2004; Gonzalez, Briones et al. 2005). Rodent cerebral vessels have also been studied in isolation, but the mechanical properties of these vessels have not been fully characterized. Emphasis has mainly been on circumferential behavior within the physiological loading range (Hajdu and Baumbach 1994; Coulson, Chesler et al. 2002; Coulson, Cipolla et al. 2004). A more complete definition of these properties is an important step toward addressing questions more specific to cerebral vessel injury and disease. Accordingly, the aim of this research was to define the biaxial and failure properties of passive rat middle cerebral arteries (MCAs) and to compare these characteristics to those of previously studied human cerebral vessels.

CHAPTER 2

METHODS

2.1 Vessel Dissection and Cannulation

The MCA was dissected from 7 male Sprague Dawley rats (370 ± 40 gm). All procedures met requirements established by the Institutional Animal Use and Care Committee at the University of Utah. Rats were euthanized via CO_2 asphyxiation and then exsanguinated via cardiac perfusion using Hank's Buffered Saline Solution (HBSS), followed by a 1% nigrosin dye (Sigma) HBSS solution. The composition of the HBSS was (concentrations in mM): KCl 5.37, KH_2PO_4 0.44, NaCl 136.9, Na_2HPO_4 0.34, D-Glucose 5.55, $NaHC0_3$ 4.17. The dye allowed for the staining of the endothelial surface of the MCA without staining of the brain tissue to enhance visibility of the artery and its branches during dissection. After removal of the MCA from the brain, a small ring was obtained from its distal end and stored in HBSS for later determination of the reference cross-sectional area. MCA side branches were ligated with individual fibrils from unwound 6-0 silk suture. The MCA was then cannulated with either 35 gauge stainless steel hypodermic needles or glass tip needles of the same tip diameter and secured with 6-0 silk suture and cyanoacrylate glue. The lack of calcium in the HBSS ensured the MCA smooth muscle would be relaxed during testing, thus ensuring passive mechanical properties.

2.2 Experimental Apparatus and Methodology

Mechanical testing methodology was similar to that described previously (Monson, Barbaro et al. 2008). Briefly, the needles on which the MCA were mounted, and the associated mounting fixtures, were attached to a vertical linear stage (Parker Automation). The upper fixture was suspended from a 250 gram capacity load cell (Sensotec Model 31) through an X-Y stage (Newport, MS-125-XY) that allowed for the correction of any needle misalignment. The lower fixture was mounted to the stage via a vertical, low friction sled supported by a voice coil actuator (Akribis MGV52-25-1.0). Movement of this voice coil moved the lower fixture vertically along the sled track, axially stretching the MCA. A narrow, clear plastic water bath filled with HBSS and surrounding the MCA and needles was attached to the lower fixture. Specimens were viewed via a digital video camera (Pixelink, PL-A641) equipped with a zoom lens (Edmund Optics, VZM 450i). Vessels were perfused with HBSS originating from a syringe attached to a linear actuator (Ultramotion, Digit) and passing through the lower fixture, the mounted MCA, and the upper fixture. Inline pressure transducers (Honeywell, MicroSwitch 26PCDFM6G) were located both proximal and distal to the mounted MCA, equidistant from the vessel. The average of these two transducer readings indicated the luminal pressure. Data and video acquisition, as well as control of the set-up, were accomplished using a custom LabVIEW program (National Instruments). Voice coil and syringe linear actuator positions were given by digital encoders (resolution 1.0 μm).

Following the mounting of the MCA, it was preconditioned and tested using methods detailed previously (Monson, Barbaro et al. 2008). In brief, after preconditioning, a test was performed to allow determination of specimen zero-load length. This was followed by a series of six subfailure biaxial sequences, three inflation

tests at various levels of axial stretch and three axial stretch tests at various levels of pressure. Finally, the vessel was stretched axially, at a constant pressure of 13.3 kPa, until it failed.

2.3 Data Analysis

Data from the encoders, load cell, and pressure transducers were recorded at 100 Hz using a custom LabVIEW program. Images recorded (3 Hz) during the fourth cycle of each test were converted into separate video files, and image analysis software (Vision Assistant, National Instruments) was used to measure vessel outer diameter in the current configuration (d_e). Since images were obtained at a lower rate than the other data recorded in LabVIEW, additional diameter data were defined using interpolation to allow one-to-one correspondence. Noise observed in the load cell readings was smoothed using the SAE J211 filter (SAE 1995).

Cross-sectional dimensions were also determined using Vision Assistant. The difference in the areas of the outer and inner contours of the unloaded specimen cross section was taken as the reference cross-sectional area (A). For elliptical cross sections, the zero-load outer diameter (D_e) was approximated as being the average of the major and minor axes. Reference configuration inner diameter (D_i) was computed from the cross-sectional area and zero-load outer diameter using the definition of cross-sectional area for a tube. Current inner diameter (d_i) was calculated by assuming incompressibility. The image corresponding to the point at which the force starts to increase from zero during the zero-load test was analyzed in Vision Assistant to attain the reference length (L). Current vessel length (l) was defined as the distance moved by the voice coil from the zero-load position, added to the zero-load length.

Vessels were assumed to be homogeneous circular cylinders such that midwall vessel stretch was computed using the following equations:

$$\boldsymbol{\lambda_\theta = \left(\frac{d_i + d_e}{D_i + D_e}\right)} \tag{2.1}$$

$$\boldsymbol{\lambda_z = \left(\frac{l}{L}\right)} \tag{2.2}$$

where the subscripts θ and z refer to the local cylindrical coordinates in the circumferential and axial directions, respectively. The mean Cauchy stresses in the circumferential (T_θ) and axial (T_z) directions were determined by enforcing equilibrium in the two directions, as follows:

$$\boldsymbol{T_\theta = p_i \left(\frac{d_i}{d_e + d_i}\right)} \tag{2.3}$$

$$\boldsymbol{T_z = \frac{\lambda_z}{A}\left(F_z + \frac{\pi}{4} p_i d_i^2\right)} \tag{2.4}$$

where p_i and F_z represent the transmural pressure and experimental axial force.

To facilitate comparison of stiffness in the axial and circumferential directions, stress–stretch data around approximate *in vivo* conditions were examined. For the circumferential direction, the stress–stretch values corresponding to a pressure of 13.3 kPa (100 mmHg) were identified in the inflation test having the lowest value of axial

stretch. These were taken as the *in vivo* values. A line was fit through the data around this point to determine stiffness. Because the value of in *vivo* stretch was not always obvious in this dataset, we assumed that the axial *in vivo* stress would have the same value as that in the circumferential direction for the same specimen. A line was then fit through this axial stress value to estimate *in vivo* axial stiffness.

A hyper-elastic constitutive model based on a phenomenological approach was applied to parameterize the biaxial (circumferential and axial) response of the vessels. Following the pseudoelasticity assumption made by Fung, we applied the following form of strain energy function with the zero-load state as the reference configuration (Fung 1993):

$$\boldsymbol{W = \frac{1}{2} c\,(e^{Q} - 1)} \tag{2.5}$$

$$\boldsymbol{Q = c_1 E_{\theta\theta}^2 + c_2 E_{zz}^2 + 2 c_3 E_{\theta\theta} E_{zz}} \tag{2.6}$$

where W represents the strain energy per unit mass of the material while $E_{\theta\theta}$ and E_{zz} refer to the Green strains in the circumferential and axial directions. Shear strains were ignored owing to the axisymmetric loading conditions and observed response. The model incorporates four material parameters c (units of stress), c_1, c_2 and c_3 (dimensionless). Incompressibility was enforced *directly* (Humphrey 2002). Differentiation of the strain energy equation leads to the following stress-strain relationships:

$$\boldsymbol{t_{\theta\theta} = t_{rr} + \lambda_{\theta}^{2} \frac{\partial W}{\partial E_{\theta\theta}}} \tag{2.7}$$

$$\boldsymbol{t_{zz} = t_{rr} + \lambda_{z}^{2} \frac{\partial W}{\partial E_{zz}}} \tag{2.8}$$

where

$$\boldsymbol{t_{rr}(r) = -P_i + \int_{r_i}^{r} \left(\lambda_{\theta}^{2} \frac{\partial W}{\partial E_{\theta\theta}}\right)\left(\frac{1}{r}\right) dr} \tag{2.9}$$

In the above equations, $t_{\theta\theta}$, t_{zz}, and t_{rr} correspond to the theoretical Cauchy stress values in the circumferential, axial, and radial directions, respectively. Mean values of $t_{\theta\theta}$ and t_{zz} were calculated for comparison to experimentally derived stresses. Material parameters c, c_1, c_2, and c_3 that best fit the experimental data were computed by employing a nonlinear regression routine (fminsearch) in MATLAB (Appendix A.1).

CHAPTER 3

RESULTS

3.1 Rat MCA Response

Seven arteries were successfully tested. Mean (± standard deviation) unloaded outer diameter and length of these specimens were $0.23\ (\pm 0.01)$ mm and $3.71\ (\pm 0.61)$ mm, respectively. Typical response is shown in Figure 3.1 and 3.2 and is qualitatively similar to what we have previously reported for biaxial behavior of human cerebral arteries.

Rat MCA stress-stretch responses in the circumferential and axial directions were similar within the physiological loading range (stretch values approximately between 1.05 and 1.15) (Figure 3.3). This material symmetry was observed in all but one specimen (R7) where the axial direction was considerably stiffer (Figure 3.4); reasons for the exception are not known. Not considering this case, ratios of axial to circumferential stiffness around *in vivo* conditions ranged from 0.85 to 1.34, with an average of 1.04, consistent with the apparent symmetry.

Best-fit material parameters in Equations 2.5 and 2.6 also suggested material symmetry in these specimens. Predicted stress values (Equations 2.7 and 2.8) were fairly similar to experimental stresses corresponding to the primary direction of loading, but predictions were less accurate in the orthogonal direction (Figure 3.5). It is also clear that

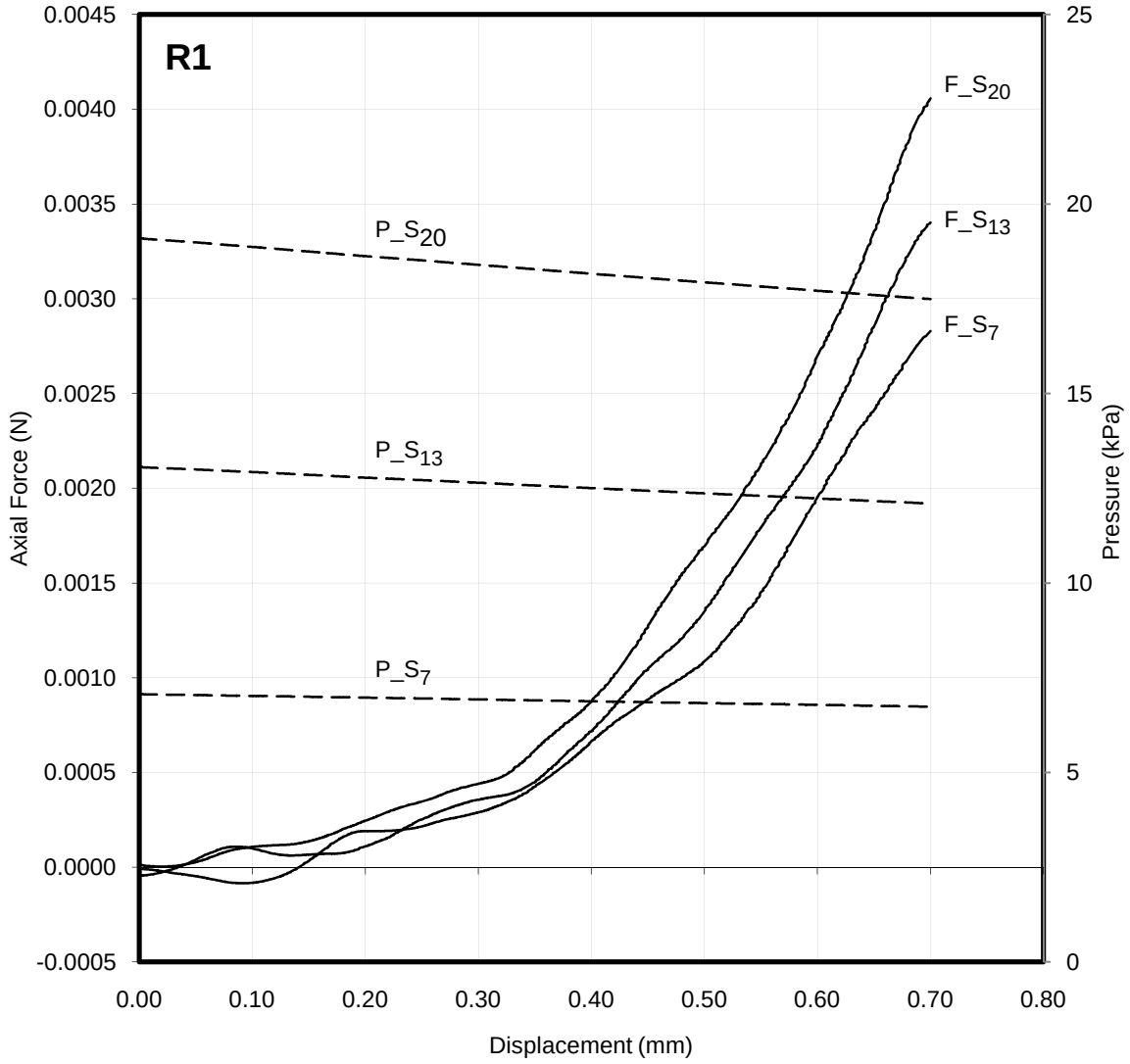

Figure 3.1: Axial force (F_S_m) and luminal pressure (P_S_m) for a representative MCA sample (R1) during axial stretch tests. Label subscript *m* indicates the luminal pressure for these axial stretch tests.

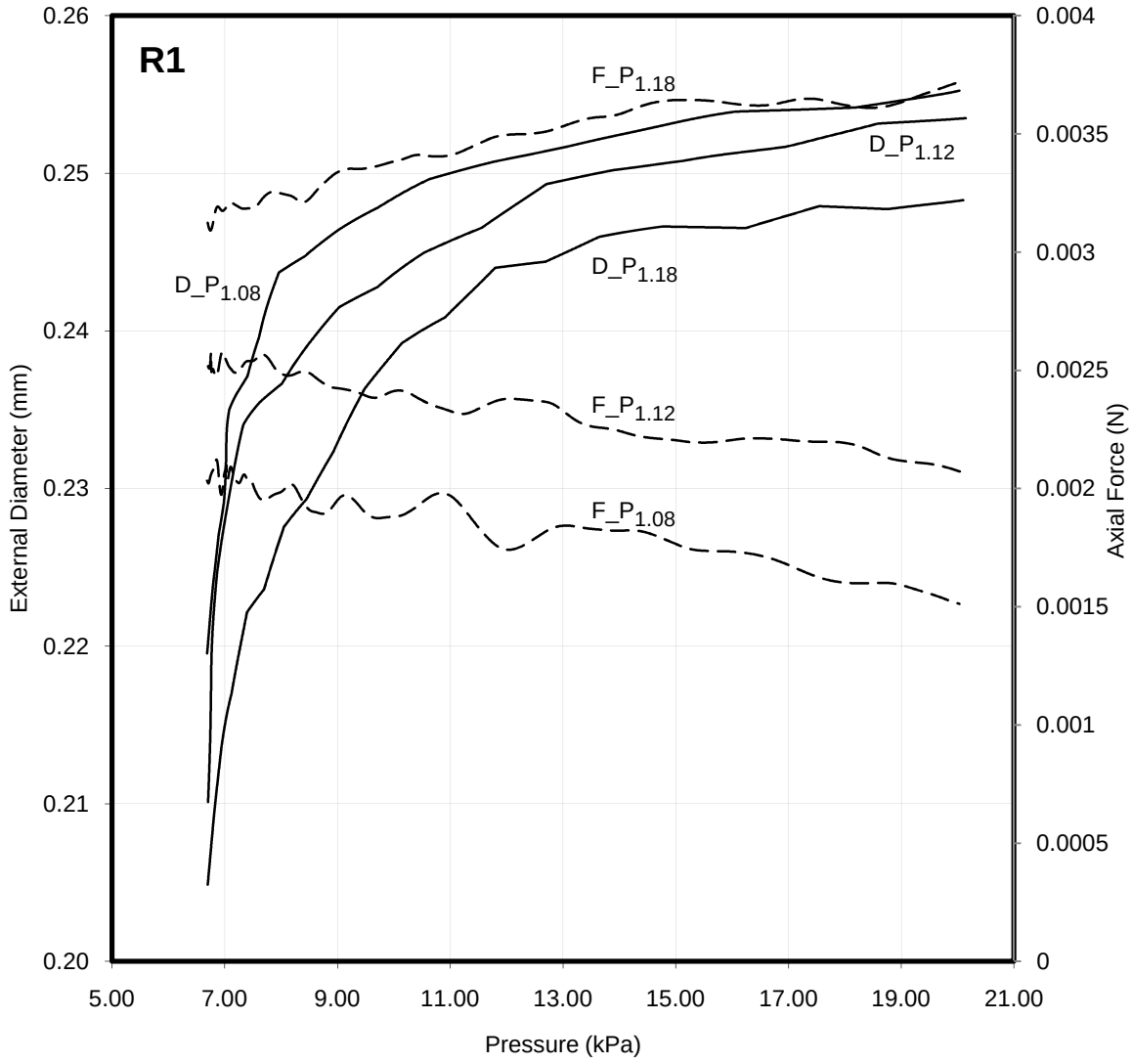

Figure 3.2: Outer diameter (D_P_n) and axial force (F_P_n) responses for a representative MCA sample (R1) during inflation tests. Label subscript *n* indicates the axial stretch for these inflation tests.

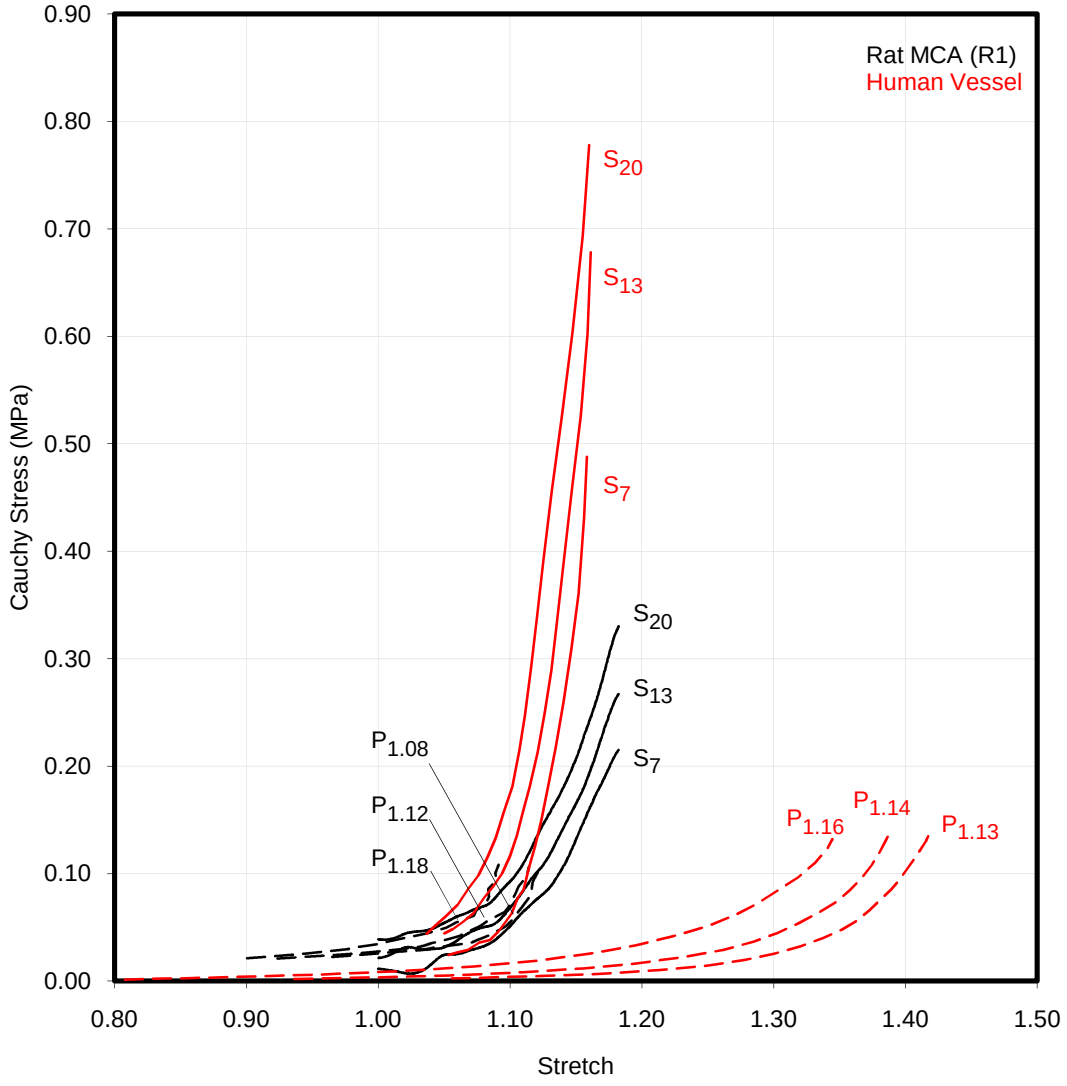

Figure 3.3: Cauchy stress-stretch response curves for representative rat MCA (R1) and human cerebral artery (Monson, Barbaro et al. 2008) samples in the axial (S_m) and circumferential (P_n) directions. Label subscript *m* indicates the luminal pressure during axial stretch tests while subscript *n* indicates the axial stretch during inflation tests.

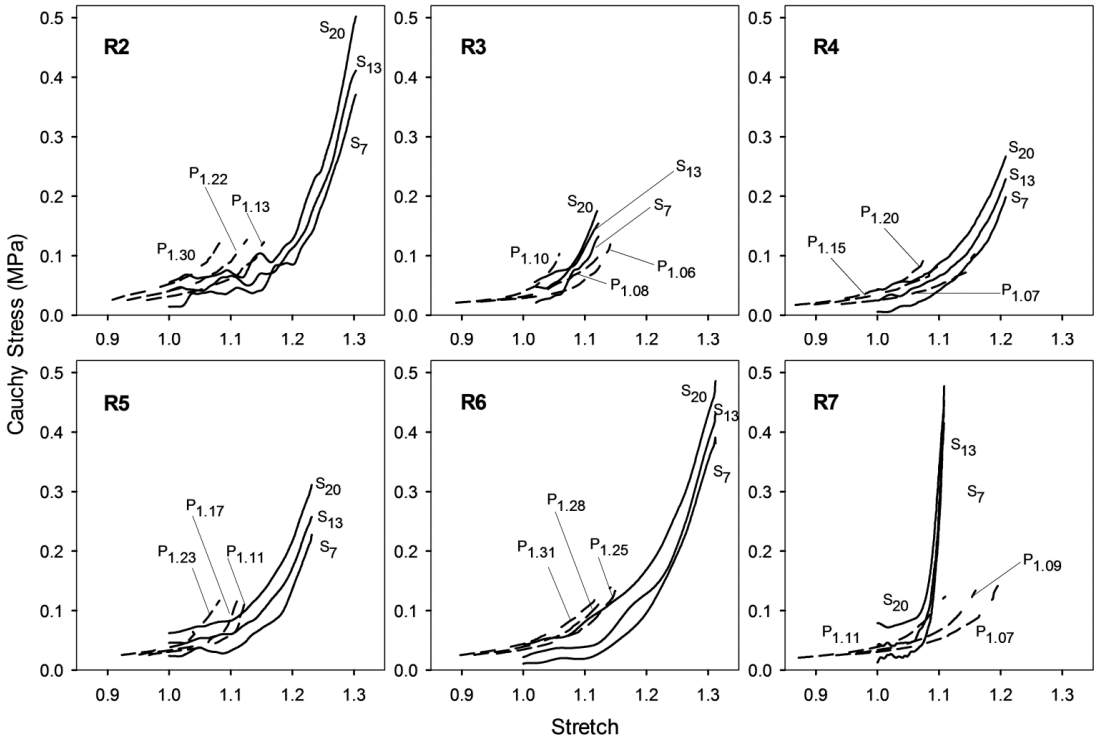

Figure 3.4: Cauchy stress-stretch response curves for remaining rat MCAs (including case in exception- R7) in the axial (S_m) and circumferential (P_n) directions. Label subscript *m* indicates the luminal pressure during axial stretch tests while subscript *n* indicates the axial stretch during inflation tests.

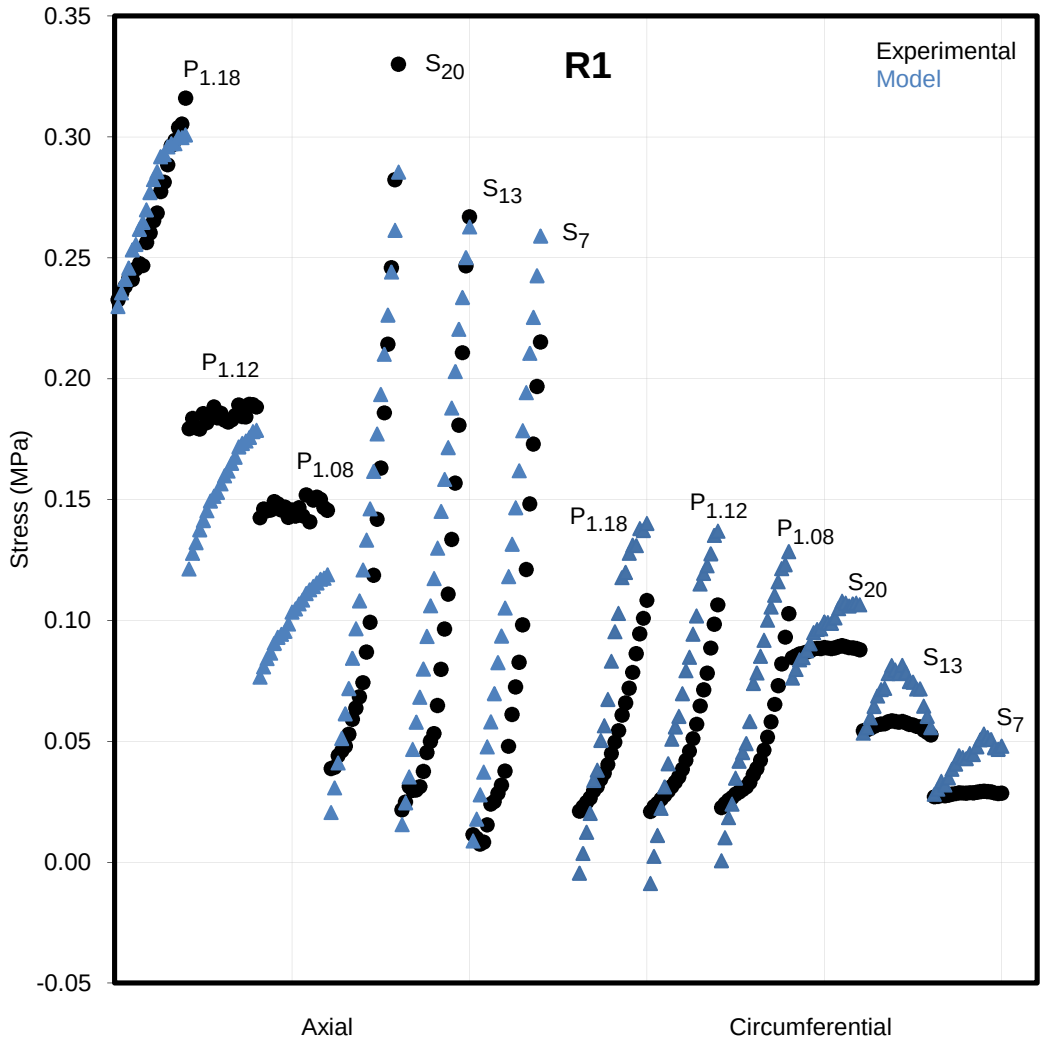

Figure 3.5: Experimental and predicted axial and circumferential stress values from the inflation (P_n) and axial (S_m) stretch tests for a representative rat MCA (R1). Label subscript *m* indicates the luminal pressure during axial stretch tests while subscript *n* indicates the axial stretch during inflation tests. Datasets having the same label are from the same test.

overall behavior was not captured well by the model, with some predicted data indicating concave-downward shapes for the primary loading direction. Despite these model shortcomings, the optimized constitutive parameters indicate that mechanical behavior in the two loading directions was similar, with the coefficients of the circumferential (c_1) and axial (c_2) strains taking on similar values in most cases (Table 3.1). Sample R7 was an exception to this where c_2 was multiple times greater than c_1. Requirements imposed by energy conservation for orthotropic symmetry in Equations 2.7 and 2.8 (c_1, c_2 , c_3 > 0 and $\sqrt{c_1 * c_2} > c_3$) were met by the determined material parameters (excepting Sample 7) (Holzapfel, Gasser et al. 2000).

3.2 Rat MCAs versus Human Cerebral Vessels

Though qualitatively similar, rat MCA behavior was notably different from that of human vessels which exhibited a marked difference between circumferential and axial responses (Figure 3.3). This is apparent both from the plotted data and from a comparison of mean material parameter values, where it is clear that the ratio of c_2 to c_1 is large for human vessels (Table 3.1). For the axial direction, stress values for human vessels are considerably larger than those for rat MCAs at comparable strains, especially beyond an axial stretch of 1.10 in the plotted case. Interestingly, for the circumferential direction, the stress values for the two types of vessel lie in a similar range, but significantly more deformation is required to reach these stresses in human vessels.

Table 3.1: Rat MCA material parameters computed for optimum fit to Equations 2.7, 2.8, 2.9 and corresponding summary of human cerebral vessels (Monson, Barbaro et al. 2008).

Rat MCAs				
Sample No.	**Material Parameters**			
	c	c_1	c_2	c_3
R1	0.67	0.68	1.32	0.29
R2	0.23	1.75	2.19	0.56
R3	0.09	5.01	7.07	2.19
R4	0.55	0.66	1.02	0.4
R5	0.15	2.57	2.84	1.12
R6	0.06	5.04	5.53	0.7
R7	0.01	14.12	72.68	-1.43
Summary				
Mean (except R7)	0.29	2.62	3.33	0.88
Std. Dev. (except R7)	0.26	2	2.44	0.71
Human Cerebral Vessels				
Summary				
Mean	4.44	7.69	174.21	-1.91
Std. Dev.	4.47	8.65	158.45	12.54

3.3 Rat MCA Failure Test Response

Failure values for the seven tested MCA samples, along with those from human cerebral vessels tested in our laboratory, are plotted in Figure 3.6. For rats, the mean value (± standard deviation) of axial stretch at failure was $1.33\ (\pm 0.11)$ while the corresponding axial 1st Piola-Kirchhoff stress (F_z/A) was $0.49\ (\pm 0.12)$ MPa. These two values for human vessels were $1.24\ (\pm 0.09)$ and $3.29\ (\pm 0.64)$ MPa, respectively. Four rat vessels failed near a suture tie-off, while three failed in midsection. Failure values were not a function of failure location (Figure 3.6). Stress values are reported in 1st Piola-Kirchhoff form because the incompressibility assumption commonly yielded a complex number for inner diameter in the current configuration, suggesting that large vessel deformations are not isochoric.

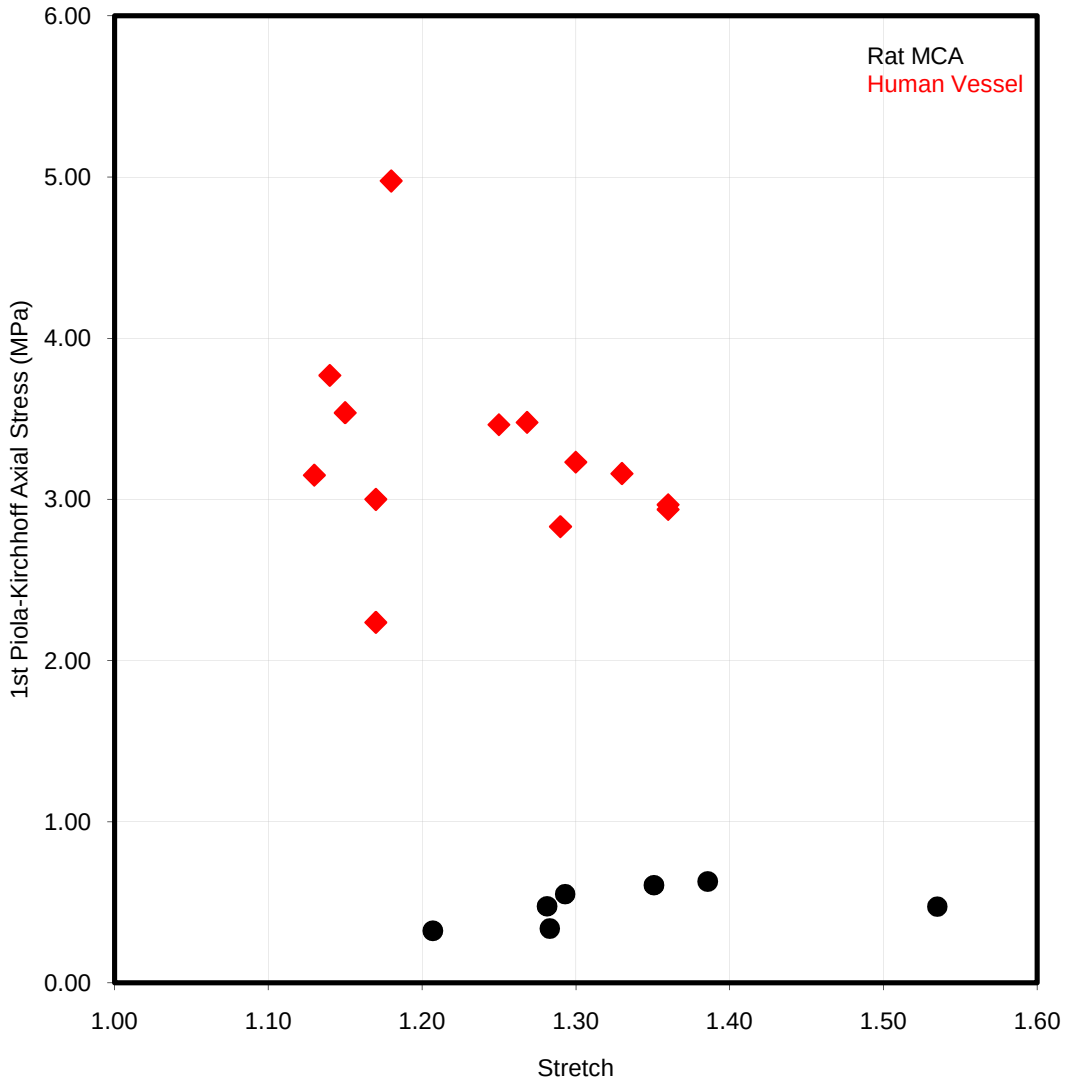

Figure 3.6: 1st Piola-Kirchhoff failure stress-stretch values for rat MCAs and human cerebral vessels.

CHAPTER 4

DISCUSSION

4.1 Summary of Findings

The present study aimed to characterize the biaxial mechanical properties of passive rat MCA and to compare them to those of human cerebral vessels. Qualitatively, the rat MCA response conformed to that of the previously studied arteries. However, some notable quantitative differences were identified with respect to material symmetry and axial stress values. Such differences should be considered in the translation of knowledge gained from rat models of TBI and stroke to the human system.

Based on the observed rat MCA stress-stretch response and the corresponding material parameter values, it is clear that behavior varies only marginally between the axial and circumferential directions, at least within the physiological loading range (for 6 of 7 specimens). This similarity was unexpected based on our previous work showing that behavior is considerably more stiff axially than circumferentially in human cerebral arteries (Monson, Barbaro et al. 2008). Reasons for these differences are unknown, but it is important to note that rat data were obtained from middle cerebral arteries while human data were collected from pial arteries on the surface of the temporal lobe, two different locations in the cerebral circulation. Our previous work comparing these two sites in humans (Monson, Goldsmith et al. 2005) indicated that differences between them were

not significant, but the comparison was made only in the axial direction. The similarity of passive behavior of MCA and pial artery in rat is also not currently known. Other dissimilarities in the general structure of rat and human cerebral arteries may also contribute to the observed differences (Lee 1995).

An additional potential reason for the observed differences in the circumferential direction could be the relatively small amount of smooth muscle in the much smaller rat MCAs. The presence of smooth muscle tone (eliminated in our testing) would be expected to shift the circumferential stress-stretch curve leftward. Given the greater amount of smooth muscle in the human vessels, this shift might be expected to be larger such that the two vessel types would have a more similar *in vivo* response, but this requires further study.

Differences between axial stress values, particularly large at failure, were also unexpected. Reasons for this disparity are unknown and should be further investigated with histological studies.

4.2 Limitations and Future Scope

The primary challenge with conducting the current experiments, relative to previous work on human vessels, was the small size of the specimens, and errors related to size could lead to some of the differences observed here. In particular, it was challenging to accurately determine reference cross-sectional characteristics since it was difficult to cut cross sections thin enough that they would consistently lie flat and open for imaging. Our measurements, however, were consistent with outer diameter measurements during testing, were similar between samples, and compare well with dimensions reported by other studies of the rat MCA (Coulson, Cipolla et al. 2004).

Another challenge with small size was force measurement. While the load cell was validated by hanging weights, forces measured were not far above its specified error levels in some tests, but results for axial stretch tests, for example, at different pressures were discernable from one another and were consistent with the multiaxial behavior observed in other vessels. In addition, filtered force traces were always compared to raw data to ensure fidelity.

As noted, the Fung-type constitutive model (Equations 2.5 and 2.6) demonstrated some significant shortcomings in fitting the collected multiaxial data. Because this project was not intended to be an investigation of constitutive models and we had previously used the Fung-type model to characterize human cerebral artery data, we utilized this model to allow comparison to the previously collected results. Other microstructure-based models (Wicker, Hutchens et al. 2008; Wagner and Humphrey 2011) that have been proposed recently would likely result in a better fit of the data, but application of the models to these data would not be expected to change the observations reported here.

Despite the significance of the stress-strain relationship in cerebrovascular mechanics, previous studies on rat cerebral vessels have mostly focused on analyzing the pressure-diameter response for different purposes (Hajdu and Baumbach 1994; Coulson, Chesler et al. 2002; Coulson, Cipolla et al. 2004). Coulson et al. have examined the rat MCA mechanical behavior in both a myogenically active state and a drug-induced passive state but they limited their study to uniaxial circumferential testing only (Coulson, Cipolla et al. 2004). Our circumferential findings compare well with theirs, i.e. the pressure-diameter relationship is nonlinear and lies within a similar range. Apart from that, other related studies have either examined rat cerebral arteries in a different state or

have focused on a different aspect. As far as we know, no researchers have conducted multiaxial testing and analysis of rat middle cerebral arteries.

While our findings shed light on the mechanical behavior of rat cerebral arteries and their relationship to those of human arteries, further work is needed to more completely define both types of vessels. In particular, the use of the zero-load state as the reference configuration ignores contributions from residual stresses (Chuong and Fung 1986). Further investigation including through-wall stress distribution is needed to better identify conditions associated with disease development and should utilize the zero-stress state as reference. With this greater detail, additional work should also address the multiple layers present in any vessel and how specific components of these layers are loaded. More advanced models, such as that proposed by Holzapfel et al. (Holzapfel, Gasser et al. 2000), that incorporate arterial microstructure and the four-fiber family model (Wicker, Hutchens et al. 2008; Wagner and Humphrey 2011) based on the strain-energy function suggested by Baek et al. (Baek, Gleason et al. 2007) should be helpful in this regard. Additionally, cerebral artery response varies with smooth muscle tone (Coulson, Cipolla et al. 2004; Wagner and Humphrey 2011), and our study focused only on passive properties. The nature of this contribution needs further attention, as do other questions related to tethering (Steelman, Wu et al. 2010) and the influence of fluid flow, in order to more completely define cerebrovasculature function in health and disease.

APPENDIX

A.1 Script to perform nonlinear regression using Levenberg Marquardt algorithm

```
[filename, pathname] = uigetfile('*.txt', 'Pick the data file');
if isequal(filename,0)|isequal(pathname,0)
    disp('File not found')
else
    disp(['File ', pathname, filename, ' found'])
end

global lamCMn lamZMn Tzz Tcc;
A = load ([pathname,filename]);
lamCMn = A(:,1);
lamZMn = A(:,2);
Tzz = A(:,3);
Tcc = A(:,4);


[filename, pathname] = uigetfile('*.txt', 'Pick the data file');
if isequal(filename,0)|isequal(pathname,0)
    disp('File not found')
else
    disp(['File ', pathname, filename, ' found'])
end

global vesConst;
B = load ([pathname,filename]);
vesConst = B(:,1);
global zlArea openAngDeg openAng refDiOut lamZ1
global refROut refRIn refRMn npts

zlArea = vesConst(2);
openAngDeg = vesConst(4);
openAng = openAngDeg * pi / 180;
refDiOut = vesConst(5);
lamZ1 = vesConst(6);

refROut = refDiOut / 2;
refRIn = sqrt(refROut^2 - zlArea * lamZ1 / openAng);
refRMn = (refROut + refRIn) / 2;

npts = length(lamZMn);
x0 = [1 1 1 1];
% Setting various options for nonlinear optimization
options = optimset('Largescale','off');
```

```
options = optimset(options,'LevenbergMarquardt','on');
options = optimset(options,'Display','iter');
options = optimset(options,'FunValCheck','on');
options = optimset(options,'MaxFunEvals',500000);
options = optimset(options,'MaxIter',500000);
options = optimset(options,'TolFun',1e-10);
options = optimset(options,'TolX',1e-8);

% Running through optimization function (fminsearch) for nonlinear
optimization using LM algorithm
[x,fval,exitflag,output] = fminsearch(@Actualobjfun3D,x0,options);
fval;
exitflag;
output;


% function that was called in the previous step
function [a] = Actualobjfun3D(x)

global lamCMn lamZMn Tzz Tcc
global vesConst
global zlArea openAngDeg openAng refDiOut lamZ1
global refROut refRIn refRMn npts

% constants used in calculation of SEF
c11 = x(1);
c12 = x(2);
c22 = x(3);
c   = x(4);

radCnt = 10;
a=0;

for place=1:npts
    rMn = openAng * lamCMn(place) / pi * refRMn;
    rIn = sqrt(rMn^2 - openAng / (lamZMn(place) * pi) * (refRMn^2 -
refRIn^2));
    rOut = sqrt(rIn^2 + openAng / (lamZMn(place) * pi) * (refROut^2 -
refRIn^2));
    Ezz = 0.5 * (lamZMn(place)^2 - 1);
    pIntSum = 0;
    i = 0;

    % step through wall thickness to determine stress values
    while i<=radCnt
        rEval = rIn + (i / radCnt) * (rOut - rIn);
        refREval = sqrt(refRIn^2 + (pi * lamZMn(place) / openAng) *
(rEval^2 - rIn^2));
        lamC = pi * rEval / (openAng * refREval);
        Ecc = 0.5 * (lamC^2 - 1);
        Qval = c11*Ecc^2 + c22*Ezz^2 + 2*c12*Ecc*Ezz;        dWdEcc = c
* exp(Qval) * (c11*Ecc + c12*Ezz);
        intVal = lamC^2 * dWdEcc / rEval ;
        dWdEzz = c * exp(Qval) * (c22*Ezz + c12*Ecc);
        if (i > 0)
```

```
        pIntSum = pIntSum + (0.5 * (intVal + intValPrev) * (rEval -
rEvalPrev)) ;          % [kPa]
        end

        intValPrev = intVal;
        rEvalPrev = rEval;

        i = i+1;
    end

    press = pIntSum;
    tccSum = 0;
    tzzSum = 0;
    pIntSum = 0;
    LIntSum = 0;
    i = 0;

    while i<=radCnt
        rEval = rIn + (i / radCnt) * (rOut - rIn);
        refREval = sqrt(refRIn^2 + (pi * lamZMn(place) / openAng) *
(rEval^2 - rIn^2));
        lamC = pi * rEval / (openAng * refREval);
        Ecc = 0.5 * (lamC^2 - 1);
        Qval = c11*Ecc^2 + c22*Ezz^2 + 2*c12*Ecc*Ezz;

        dWdEcc = c * exp(Qval) * (c11*Ecc + c12*Ezz);
        intVal = lamC^2 * dWdEcc / rEval ;
        dWdEzz = c * exp(Qval) * (c22*Ezz + c12*Ecc);
        LIntVal = (2 * lamZMn(place)^2 * dWdEzz - lamC^2 * dWdEcc) *
rEval ;

        if (i > 0)
            pIntSum = pIntSum + (0.5 * (intVal + intValPrev) * (rEval -
rEvalPrev)) ;
            LIntSum = LIntSum + (0.5 * (LIntVal + LIntValPrev) * (rEval
- rEvalPrev));
        end

        trr = (-1) * press + pIntSum ;
        tcc = trr + lamC^2 * dWdEcc ;
        tzz = trr + lamZMn(place)^2 * dWdEzz ;

        tccSum = tccSum + tcc ;
        tzzSum = tzzSum + tzz ;

        intValPrev = intVal ;
        LIntValPrev = LIntVal ;

        rEvalPrev = rEval ;

        i = i+1;
    end

    load = pi * LIntSum;
    tccMn(place) = tccSum / (radCnt + 1);
```

```
    tzzMn(place) = tzzSum / (radCnt + 1);
    tzzMnComp(place) = load / (openAng * (refROut^2 - refRIn^2));
    a=a+(tccMn(place)-Tcc(place))^2+(tzzMn(place)-Tzz(place))^2;

end
```

REFERENCES

Baek, S., R. L. Gleason, et al. (2007). "Theory of small on large: Potential utility in computations of fluid-solid interactions in arteries." Computer Methods in Applied Mechanics and Engineering **196**(31-32): 3070-3078.

Busby, D. E. and A. C. Burton (1965). "The effect of age on the elasticity of the major brain arteries." Canadian Journal of Physiology and Pharmacology **43**: 185-202.

Chuong, C. J. and Y. C. Fung (1986). "On residual stresses in arteries." Journal of Biomechanical Engineering **108**(2): 189-92.

Coulson, R. J., N. C. Chesler, et al. (2002). "Effects of ischemia and myogenic activity on active and passive mechanical properties of rat cerebral arteries." American Journal of Physiology - Heart and Circulatory Physiology **283**(6): H2268-75.

Coulson, R. J., M. J. Cipolla, et al. (2004). "Mechanical properties of rat middle cerebral arteries with and without myogenic tone." Journal of Biomechanical Engineering **126**(1): 76-81.

Faul, M., L. Xu, et al. (2010). Traumatic Brain Injury in the United States: Emergency Department Visits, Hospitalizations and Deaths 2002–2006. Atlanta, GA, Centers for Disease Control and Prevention, National Center for Injury Prevention and Control.

Fung, Y. C. (1993). Biomechanics: Mechanical Properties of Living Tissues. New York, Springer.

Gonzalez, J. M., A. M. Briones, et al. (2005). "Influence of elastin on rat small artery mechanical properties." Experimental Physiology **90**(4): 463-8.

Hajdu, M. A. and G. L. Baumbach (1994). "Mechanics of large and small cerebral arteries in chronic hypertension." American Journal of Physiology **266**(3 Pt 2): H1027-33.

Hayashi, K., S. Nagasawa, et al. (1980). "Mechanical properties of human cerebral arteries." Biorheology **17**(3): 211-8.

Hogestatt, E. D., K. E. Andersson, et al. (1983). "Mechanical properties of rat cerebral arteries as studied by a sensitive device for recording of mechanical activity in isolated small blood vessels." Acta Physiologica Scandinavica **117**(1): 49-61.

Holzapfel, G., T. Gasser, et al. (2000). "A new constitutive framework for arterial wall mechanics and a comparative study of material models." Journal of Elasticity **61**(1): 1-48.

Humphrey, J. D. (2002). Cardiovascular Solid Mechanics: Cells, Tissues, and Organs. New York, Springer.

Lee, R. M. (1995). "Morphology of cerebral arteries." Pharmacology & Therapeutics **66**(1): 149-73.

Lloyd-Jones, D., R. J. Adams, et al. (2010). "Heart disease and stroke statistics--2010 update: a report from the American Heart Association." Circulation **121**(7): e46-e215.

Monson, K. L., N. M. Barbaro, et al. (2008). "Biaxial response of passive human cerebral arteries." Annals of Biomedical Engineering **36**(12): 2028-41.

Monson, K. L., W. Goldsmith, et al. (2005). "Significance of source and size in the mechanical response of human cerebral blood vessels." Journal of Biomechanics **38**(4): 737-44.

Rosamond, W., K. Flegal, et al. (2008). "Heart disease and stroke statistics--2008 update: a report from the American Heart Association Statistics Committee and Stroke Statistics Subcommittee." Circulation. **117:** e25-146.

SAE (1995). S.A.E. Instrumentation for Impact Test. Part 1: Electronic Instrumentation, SAE J211-1. Warrendale, PA, Society of Automotive Engineers.

Scott, S., G. G. Ferguson, et al. (1972). "Comparison of the elastic properties of human intracranial arteries and aneurysms." Canadian Journal of Physiology and Pharmacology **50**(4): 328-32.

Steelman, S. M., Q. Wu, et al. (2010). "Perivascular tethering modulates the geometry and biomechanics of cerebral arterioles." Journal of Biomechanics **43**(14): 2717-21.

Wagner, H. P. and J. D. Humphrey (2011). "Differential passive and active biaxial mechanical behaviors of muscular and elastic arteries: basilar versus common carotid." J Biomech Eng **133**(5): 051009.

Wicker, B. K., H. P. Hutchens, et al. (2008). "Normal basilar artery structure and biaxial mechanical behaviour." Computer Methods in Biomechanics and Biomedical Engineering **11**(5): 539-51.